Ejection Force of Tubular Injection Moldings. Part II: A Prediction Model

A.J. Pontes, A.S. Pouzada
Institute for Polymers and Composites (IPC), Department of Polymer Engineering, University of Minho, 4800-058 Guimarães, Portugal

R. Pantani, G. Titomanlio
Department of Chemical and Food Engineering, University of Salerno, 84084 Fisciano (SA), Italy

The integrated knowledge of the injection molding process and the material changes induced by processing is essential to guarantee the quality of technical parts. In the case of parts with deep cavities, quite often the ejection phase of the molding cycle is critical. Thus, in the mold design stage, the aspects associated with the ejection system will require special consideration. In particular, the prediction of the ejection force will contribute to optimizing the mold design and to guarantee the integrity of the moldings. In this work, a simulation algorithm based on a thermomechanical model is described and their predictions are compared with experimental data obtained from a fully-instrumented mold (pressure, temperature, and force). Three common thermoplastics polymers were used for the tubular moldings: a semicrystalline polypropylene and two amorphous thermoplastics: polystyrene and polycarbonate. The thermomechanical model is based on the assumption of the polymer behavior changing from purely viscous to purely elastic below a transition point. This point corresponds to solidification determined by temperature in the case of amorphous materials and by critical crystallinity for semicrystalline polymers. The model results for the ejection force closely agree with the experimental data for the three materials used.

INTRODUCTION

In an injection mold, the ejection system must operate in a way that provides a balanced operation without damaging the molding or the ejector components. Hence, during the mold design, the estimation of the ejection forces is essential.

One approach to predict the ejection force in simple geometries [1–3], such as sleeves, consists of calculating the ejection force by multiplying the contact pressure, p_c, acting on the core surface, the contact area, A_c, and the coefficient of friction (μ) at ejection time between plastic and steel:

$$\mathrm{Fe} = \mu \cdot p_c \cdot A_c \tag{1}$$

This principle is followed in the technical literature for mold design (e.g., Menges and Mohren [4]).

An important factor in ejection is the static coefficient of friction between the plastic and metal surfaces in contact. Menges and Bangert [5] in the early 1980s were the first to develop a mold suitable to measure the coefficient of static friction in conditions identical to those occurring at the ejection. In their study, it was demonstrated that the static coefficient of friction is greatly influenced by the surface roughness, contact temperature, and some processing variables such as cooling time, melt temperature, and holding pressure. More recently Wang et al. [6] proposed a numerical approach to predict the ejection forces and to optimize the layout of ejector pins, based on thermal stress calculations [7]. Special attention was given to the proper modeling of the thermal condition during the injection molding, namely to verify if the assumption of a constant mold temperature and "perfect contact condition" was valid.

This article reviews the theoretical aspects associated to the ejection forces in injection molding. Using the same approach as Titomanlio and Jansen [8, 9] to develop a thermomechanical model to predict the shrinkage in injection molded plates, a model is developed to calculate the shrinkage and ejection forces in tubular moldings. The predictions are compared with experimental data already detailed in Part I of this article [10]

Correspondence to: A.S. Pouzada; e-mail: asp@dep.uminho.pt
Contract grant sponsor: IC-PME Programme to the Mouldforce Project; contract grant number: P0015.

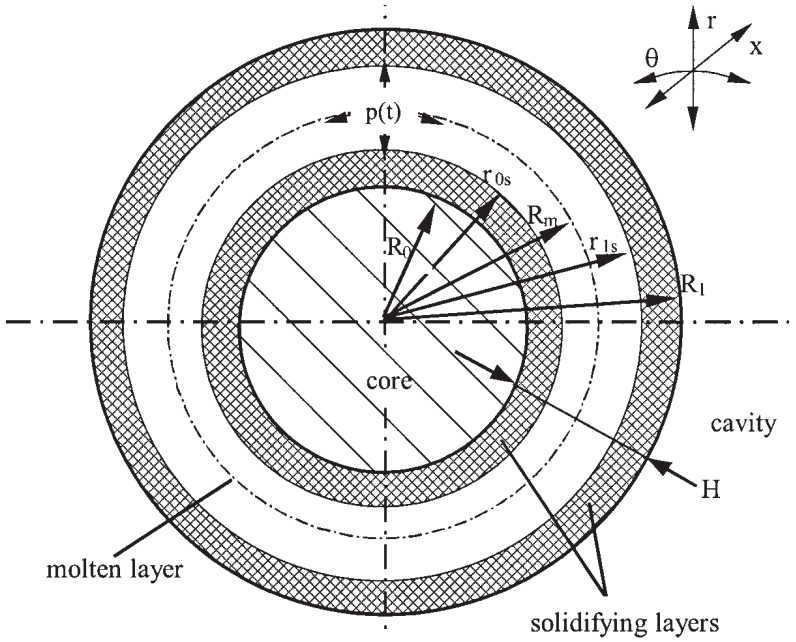

FIG. 1. Schematic cross-section of the solidifying tube.

THEORY

Stress Field Before Ejection

Consider a very thin tube, in relation to diameter, of thickness H that is cooled from the inside and the outside. Let r be the radial coordinate, ranging from R_0 at the internal surface to R_1 at the external surface, θ the angular coordinate, and x the longitudinal coordinate of the tube (Fig. 1).

The solidifying tube consists of two solid layers, with molten polymer between them. It is assumed that there is thermal symmetry in relation to R_m (average radius) and a uniform temperature profile in the tangential direction (across flow). The positions of the solid-melt interfaces are indicated as $r_{0s}(r,t)$ and $r_{1s}(r,t)$, at each instant before complete solidification.

Assumptions

In addition to the assumptions of a thin walled tube and solidification symmetry with respect to the average radius, R_m, the following assumptions are considered:

1. Continuity of stress and strain at the solid-melt interface.
2. The tangential stress, $\sigma_{\theta\theta}$, is independent from the angular coordinate θ.
3. The radial stress, σ_{rr}, is independent from the radial coordinate, r.
4. The shear components can be neglected in the solidified layer ($\tau_{\theta x} = \tau_{xr} = \tau_{\theta r} = 0$ and $\gamma_{\theta x} = \gamma_{xr} = \gamma_{\theta r} = 0$).
5. The deformation of the solidified layer is uniform (the deformation in the θ and x directions do not depend on r).
6. No warpage occurs during solidification, i.e., the planes perpendicular to the tube axis remain plane during solidification.
7. The solid polymer is elastic, whereas the melt is considered unable to withstand relevant tensile stresses [11, 12].
8. The frozen-in flow-induced stresses can be neglected (flow-induced stresses are typically one order of magnitude lower than the thermal-pressure induced stresses [13]).
9. Temperature, pressure, position of solid-melt interface and crystallization status are known at each instant.

The stresses σ_{ii} and strains ϵ_{ii} (i = x, θ, r) can be obtained in cylindrical coordinates from Hooke's law [14, 15].

Accordingly the stress components for the solid layer can be written as

$$\sigma_{xx} = \frac{E}{1-\nu^2}[\varepsilon_{xx} + \nu\varepsilon_{\theta\theta}] - \frac{\nu}{1-\nu}p(x,t)$$

$$\sigma_{\theta\theta} = \frac{E}{1-\nu^2}[\varepsilon_{\theta\theta} + \nu\varepsilon_{xx}] - \frac{\nu}{1-\nu}p(x,t) \qquad (2)$$

$$\sigma_{rr} = -p(x,t)$$

or, more briefly

$$\sigma_{xx} = S_{xx}(x, r, t) - p(x,t)$$

$$\sigma_{\theta\theta} = S_{\theta\theta}(x, r, t) - p(x,t) \qquad (3)$$

$$\sigma_{rr} = -p(x,t)$$

where

$$S_{xx} = \frac{\mathrm{E}}{1-\nu^2}(\varepsilon_{xx}^{obs} + \nu\varepsilon_{\theta\theta}^{obs}) - \frac{\mathrm{E}}{1-\nu}(\varepsilon_{xx}^{T} + \varepsilon^{p})$$

$$S_{\theta\theta} = \frac{\mathrm{E}}{1-\nu^2}(\varepsilon_{\theta\theta}^{obs} + \nu\varepsilon_{xx}^{obs}) - \frac{\mathrm{E}}{1-\nu}(\varepsilon_{\theta\theta}^{T} + \varepsilon^{p}) \qquad (4)$$

$$S_{rr} = 0$$

p(x,t) being the melt pressure.

The strain field is described in terms of an observable strain, a thermal dependent strain and a pressure dependent strain:

$$\varepsilon_{ii} = \varepsilon_{ii}^{obs} - \varepsilon_{ii}^{T} - \varepsilon^{p} \qquad (5)$$

All the components of the strain are dependent on the coordinate x and on time, t.

The strains are related to the displacements in the radial direction, u, and in the longitudinal direction, w, in the following way:

$$\varepsilon_{rr}^{obs}(x, r, t) = \frac{du}{dr}$$

$$\varepsilon_{\theta\theta}^{obs}(x, r, t) = \frac{u}{r}$$

$$\varepsilon_{xx}^{obs}(x, r, t) = \frac{dw}{dr}.$$

The stress distribution is evaluated after each time interval, dt. After differentiation of *Eq. 4* with respect to time, it results in:

$$\dot{S}_{\theta\theta} = \frac{\mathrm{E}}{1-\nu^2}(\dot{\varepsilon}_{\theta\theta}^{obs} + \nu\dot{\varepsilon}_{xx}^{obs}) - \frac{\mathrm{E}}{1-\nu}\left(\frac{1}{3\cdot \mathrm{v}}\dot{\mathrm{v}}\right) \qquad (6)$$

the dot denoting derivation with respect to time, and

$$\dot{\varepsilon}_{xx}^{T} + \dot{\varepsilon}^{p} = \dot{\varepsilon}_{\theta\theta}^{T} + \dot{\varepsilon}^{p} = \alpha\cdot\dot{T} - \beta\cdot\dot{p} = \frac{1}{3\cdot \mathrm{v}}\dot{\mathrm{v}}.$$

During the solidification process inside the mold, the molding will be considered as constrained in the flow direction (zero shrinkage in the mold). However, it is allowed to shrink in the thickness direction as soon as the pressure in the cavity side vanishes.

The strain in the thickness direction, as derived from Hooke's law, and considering $\sigma_{rr} = -p$(x,t) is given by

$$\varepsilon_{rr}^{obs} = \frac{1+\nu}{1-\nu}\left(\frac{\partial \mathrm{v}}{3\cdot \mathrm{v}}\right) - \frac{\nu}{1-\nu}(\varepsilon_{\theta\theta}^{obs} + \varepsilon_{xx}^{obs}). \qquad (7)$$

The through-thickness shrinkage must be evaluated as from its onset at $\mathrm{t} = \mathrm{t}_{\mathrm{r}}^{*}$. $\mathrm{t}_{\mathrm{r}}^{*}$ is determined from the condition:

$$p(t_r^{*}) = 0.$$

The through-thickness shrinkage until ejection is determined by considering the strains in both solid (*Eq. 7*) and molten layers

$$\text{(solid)} \quad \varepsilon_{rr,solid}^{obs} = \frac{1+\nu}{1-\nu}\int_{t_r^{*}}^{t_e}\frac{1}{3\mathrm{v}}\dot{\mathrm{v}}dt - \frac{\nu}{1-\nu}(\varepsilon_{\theta\theta}^{obs} + \varepsilon_{xx}^{obs})\Big|_{t_r^{*}}^{t_e}$$

$$\text{(molten)} \quad \varepsilon_{rr,molten}^{obs} = \int_{t_r^{*}}^{t_e}\frac{1}{3\mathrm{v}}\dot{\mathrm{v}}\cdot dt.$$

At the start of the thickness shrinkage, $\mathrm{t}_{\mathrm{r}}^{*}$, the reference dimensions coincide with the mold dimensions. Considering symmetry in relation to the average radius ($\mathrm{R_m}$) the thickness shrinkage $\mathrm{Sh_r}$(x,t) is obtained by integrating $\varepsilon_{rr}^{obs}(x, r, t)$ from the internal surface, $\mathrm{R_0}$, of the tube to its average radius, $\mathrm{R_m}$:

$$\mathrm{Sh_r}(x, t)\Big|_{t_r^{*}}^{t_e} = -\frac{1}{\mathrm{R_m} - \mathrm{R_0}} \times \left(\int_{\mathrm{R_0}}^{\mathrm{r_{0s}}}\varepsilon_{rr\ solid}^{obs}\cdot dr + \int_{\mathrm{r_{0s}}}^{\mathrm{R_m}}\varepsilon_{rr\ melt}^{obs}\cdot dr\right)\Big|_{t_r^{*}}^{t_e}. \qquad (8)$$

The shrinkage in the thickness direction causes strain changes in the tangential direction.

After $\mathrm{t}_{\mathrm{r}}^{*}$, the cross section dimensions of the shrinking part will be dependent on time, as follows:

External radius $\quad \mathrm{R_{1,part}(t)} < \mathrm{R_1}$

Average radius $\quad R_{m,part}(t) = \dfrac{R_{1,part}(t) + R_0}{2} < R_m$

Internal radius $\quad \mathrm{R_0} = \text{constant}$

and

Part thickness $\quad H_{part}(t) = R_{1,part}(t) - R_0 < R_1 - R_0 = H$

where H is the thickness of the mold impression.

Thus the tangential strain at each moment is

$$\varepsilon_{\theta\theta}^{obs} = -\frac{\pi\cdot R_m - \pi\cdot R_{m,part}}{\pi\cdot R_m} = -\frac{R_1 + R_0 - R_{1,part} - R_0}{R_1 + R_0} = -\frac{R_1 - R_{1,part}}{2\cdot R_m} \qquad (9)$$

and the thickness shrinkage

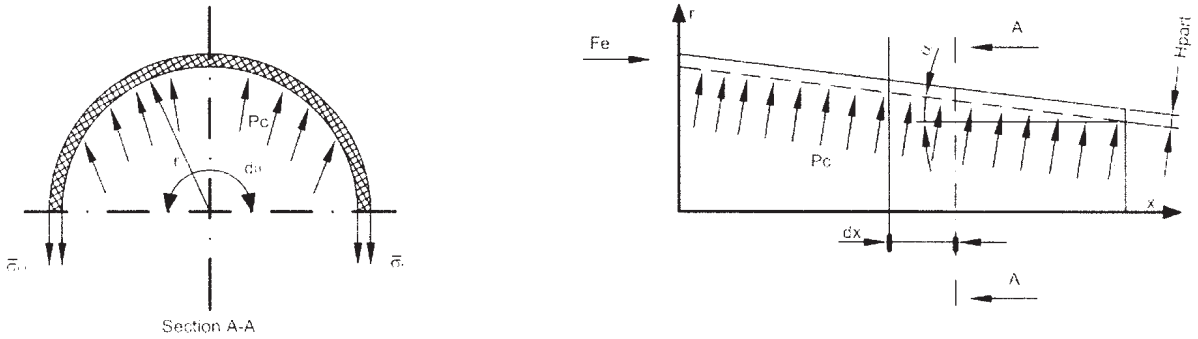

FIG. 2. Diagram of force balance before ejection.

$$\varepsilon_{rr}^{obs} = -Sh_r = -\frac{H - H_{part}}{H} = -\frac{R_1 - R_0 - R_{1,part} + R_0}{H} = -\frac{R_1 - R_{1,part}}{H}. \quad (10)$$

Substituting *Eq. 10* into *Eq. 9*, the relation between the shrinkage in the thickness direction and the strain changes in the tangential direction at each moment are related as:

$$\varepsilon_{\theta\theta}^{obs}(x, t) = \frac{\mathrm{H}}{2 \cdot R_m} \varepsilon_{rr}^{obs}(x, t)$$

Consequently, from the shrinkage onset, t_r^*, until ejection

$$\varepsilon_{\theta\theta}^{obs}(x, t)\Big|_{t_r^*}^{t_e} = -\mathrm{Sh}_r(x, t)\Big|_{t_r^*}^{t_e} \frac{\mathrm{H}}{2 \cdot R_m}. \quad (11)$$

Considering that until ejection, $\dot{\varepsilon}_{xx}^{obs} = 0$ by integrating *Eq. 6* over time from the moment of the solidification of the first layer, it results for the stress distribution before ejection:

$$S_{\theta\theta}(x, r, t) = -\int_{t_{s0}}^{t} \frac{\mathrm{E}}{1 - \nu} \frac{1}{3 \cdot \mathrm{v}} \dot{\mathrm{v}} \cdot dt + \int_{t_r^*}^{t} \frac{\mathrm{E}}{1 - \nu^2} \varepsilon_{\theta\theta}^{obs} \cdot dt. \quad (12a)$$

It must be noted that $\varepsilon_{\theta\theta}^{obs} = 0$ as from the moment of solidification of the first layer, t_{s0}, until the start of thickness shrinkage, t_r^*.

An equation similar to *Eq. 12a* can be written for the *x*-direction by interchanging the subscripts θ and x, and multiplying the observable strain $\dot{\varepsilon}_{\theta\theta}^{obs}$ by Poisson's ratio.

$$S_{xx}(x, r, t) = -\int_{t_{s0}}^{t} \frac{\mathrm{E}}{1 - \nu} \frac{1}{3 \cdot \mathrm{v}} \dot{\mathrm{v}} \cdot dt + \int_{t_r^*}^{t} \frac{\nu \cdot \mathrm{E}}{1 - \nu^2} \varepsilon_{\theta\theta}^{obs} \cdot dt. \quad (12b)$$

Ejection Force

Consider the element of the tube represented in Fig. 2. It is to remark that there is a slight variation in the diameter resulting from the draft angle, α, that moldings of this type obligatory must have.

At the instant of ejection there is a pressure field, p_c, acting in the internal surface of the tube.

Making the force balance in the radial direction, it results for a radial element of amplitude $d\theta$ and length dx, at the coordinate x:

$$\frac{p_c(x)}{\cos(\alpha)} \cdot d\theta \cdot r(x) \cdot dx - 2 \cdot \overline{\sigma_{\theta\theta}}(x, t_e) \cdot H_{part} \cdot dx \cdot \sin\left(\frac{d\theta}{2}\right) = 0$$

As $\sin\left(\frac{d\theta}{2}\right) \approx \frac{d\theta}{2}$ it results

$$p_c(x) = \frac{\overline{\sigma_{\theta\theta}}(x, t_e) \cdot H_{part} \cdot \cos(\alpha)}{r(x)} \quad (13)$$

where $\overline{\sigma_{\theta\theta}}(x,t_e)$ is the average tangential stress before ejection.

When the tube is ejected from the mold core, as shown schematically in Fig. 2, the ejection force, F_e, can be obtained by the force balance between the component of friction force, μN (where μ is the coefficient friction which is considered here as a constant), and the component of the normal force, N, obtained by integrating the contact pressure, p_c, over the total contact area between the tube and the core.

Thus, the balance of the force acting in the axis direction, x, is

$$F_e = \mu \mathrm{N} \cos\alpha - \mathrm{N} \cdot \sin\alpha = N(\mu \cdot \cos\alpha - \sin\alpha) = N \cdot \cos\alpha(\mu - \tan\alpha) \quad (14)$$

with

$$\mathrm{N} = \int p_c \cdot dA \quad (15)$$

where dA is the elementary area of integration given by

TABLE 1. Molding program.*

Material	T_{inj} (°C)	T_w (°C)	P_h (MPa)	t_h (s)	t_a (s)
PC	310	85	12,40,68,89,110	10	15
PS	230	52	5,26,47, 68	8	15
PS	230	52	47	8	5,10,15,25,35
PP	210	50	5,19,33,40, 47	13	10
PP	210	50	40	13	5,10,20,30,40

*The listed pressures are the actual pressure measure in the nozzle. T_{inj}, injection temperature; T_w, mold temperature; P_h, holding pressure; t_h, holding time; t_a, time after holding phase.

$$dA = \frac{2 \cdot \pi \cdot r(x) \cdot dx}{\cos(\alpha)}. \quad (16)$$

Substituting into *Eq. 15* the corresponding value of the elementary area (*Eq. 16*) where the contact pressure is applied and its corresponding function (*Eq. 13*), results in

$$N = 2 \cdot \pi \cdot H_{part} \cdot \int_o^L \overline{\sigma_{\theta\theta}}(x, t_e) \cdot dx. \quad (17)$$

Substituting into *Eq. 14* the corresponding value of N from *Eq. 17*, it results in

$$F_e = \cos\alpha \cdot (\mu - \tan\alpha) \cdot 2 \cdot \pi \cdot H_{part} \cdot \int_o^L \overline{\sigma_{\theta\theta}}(x, t_e) \cdot dx. \quad (18)$$

The average tangential stress before ejection, $\overline{\sigma_{\theta\theta}}(x, t_e)$, is obtained substituting *Eq. 11* into *Eq. 12a* and averaging it over the thickness. In this analysis it is considered that the modulus of the polymer is constant and equal to the modulus at the average ejection temperature, $E(\overline{T_e})$, and the melt pressure at ejection, $p(x,t_e)$, is zero. Thus

$$\overline{\sigma_{\theta\theta}}(x, t_e) = -\frac{E(\overline{T_e})}{1-\nu} \int_{t_{s0}}^{t_e} \overline{\frac{1}{3 \cdot v}\dot{v}} \cdot dt - \frac{E(\overline{T_e})}{1-\nu^2} \frac{H}{2 \cdot R_m} Sh_r(t) \Big|_{t_r^*}^{t_e}. \quad (19)$$

After integration

$$\overline{\sigma_{\theta\theta}}(x, t_e) = -\frac{E(\overline{T_e})}{1-\nu} \frac{1}{3} \cdot \overline{\ln\left(\frac{v(x, r, t_e)}{v_s(x, r)}\right)} - \frac{E(\overline{T_e})}{1-\nu^2} \frac{H}{2 \cdot R_m} Sh_r(t) \Big|_{t_r^*}^{t_e}. \quad (20)$$

The function $v_s(x,r)$ is the specific volume at the moment of solidification.

Substituting *Eq. 20* into *Eq. 18* it follows that

$$F_e = \cos\alpha \cdot (\mu - \tan\alpha) \cdot \frac{2 \cdot \pi \cdot H_{part}}{1-\nu} \cdot E(\overline{T_e}) \cdot \int_o^L \left(-\frac{1}{3} \cdot \overline{\ln\left(\frac{v(x, r, t_e)}{v_s(x, r)}\right)} - \frac{H}{(1+\nu) \cdot 2 \cdot R_m} Sh_r(t) \Big|_{t_r^*}^{t_e} \right) \cdot dx. \quad (21)$$

The expression in *Eq. 21* indicates that the ejection force is directly dependent on the elastic modulus at ejection temperature, the coefficient of friction (considered here as a constant), the thickness of the part, and the variation of the (average) volume shrinkage between solidification and the ejection time.

The last term inside the integral is included if the tube shrinks in the thickness direction. This may happen for lower holding pressures or times leading to the reduction of the force required to eject the part.

EXPERIMENTAL

Molding

The experimental data used in this study were already detailed in the Part I of this study [10] and in Ref. 16, where materials and equipment were presented.

For the following discussion, the processing conditions mentioned in Table 1 were considered.

The moldings will be identified by a code, corresponding to the material and processing variables used. For example, the following code corresponds to a polypropylene molding (PP), PP.230.20.10.15, in which

- The first number refers to the injection temperature given by the thermocouple in the nozzle (230°C);
- The second number indicates the pressure applied during the holding phase measured by the pressure transducer in the nozzle (20 MPa);
- The third number indicates for how long the holding pressure is applied (10 s);
- The fourth number gives the time from the end of holding stage until the mold opening (15 s).

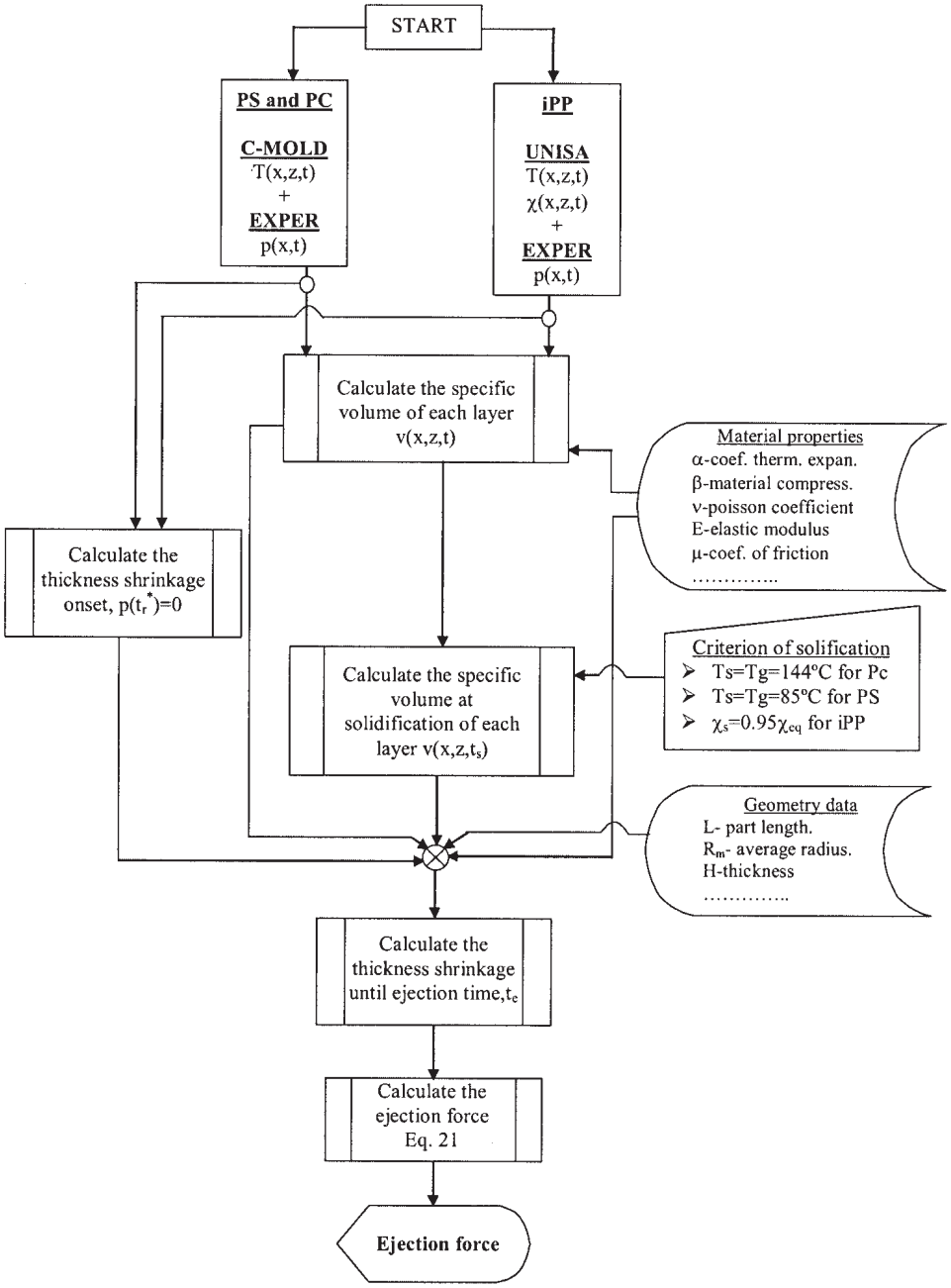

FIG. 3. Sequence of the solution process of the thermomechanical model and the input data to predict the ejection force.

RESULTS AND DISCUSSION

Analysis

Ejection force predictions were obtained using the thermomechanical model already described in the Theory section. In Fig. 3, the main steps involved in the computation of the ejection force predictions and the inputs are presented.

The input data for the ejection force model, namely the temperature, degree of crystallinity and corresponding density curves were obtained from the UNISA program [17] in the case of polypropylene (PP), and from the C-Mold program [18] for polycarbonate (PC) and polystyrene (PS).

From the input data and the material properties, the specific volume of each layer, v(x,z,t), is calculated. Then, as it was done for the shrinkage prediction, the specific volume at solidification of each layer, $v(x,z,t_s)$ is calculated using the degree of crystallinity as the criterion of solidification for the case of PP, and the glass transition temperature for the case of PC and PS.

Depending on the thickness shrinkage occurring inside the mold or after the mold opening, which is described by the condition $p(t_r^*) = 0$, the ejection force is calculated including, or not including the thickness shrinkage using *Eq. 19*.

For the calculation of the ejection force the static coefficient of friction (μ) was estimated as 0.3 for PC [6], 0.2 for PS, and 0.18 for PP. Nevertheless, the coefficient of friction

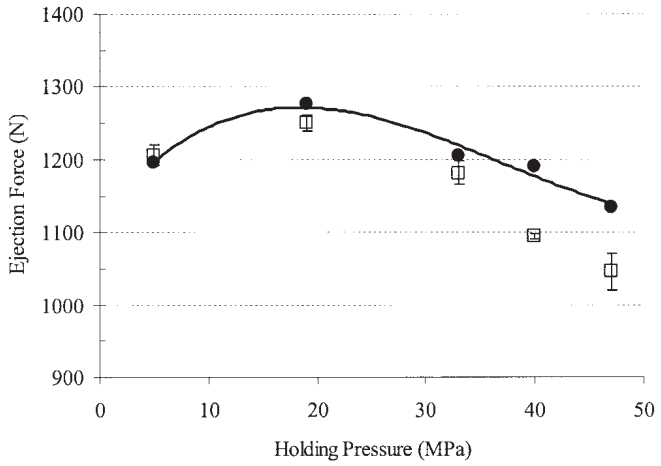

FIG. 4. Comparison of the experimental (symbols) and predicted (line) ejection force for PP. Effect of holding pressure.

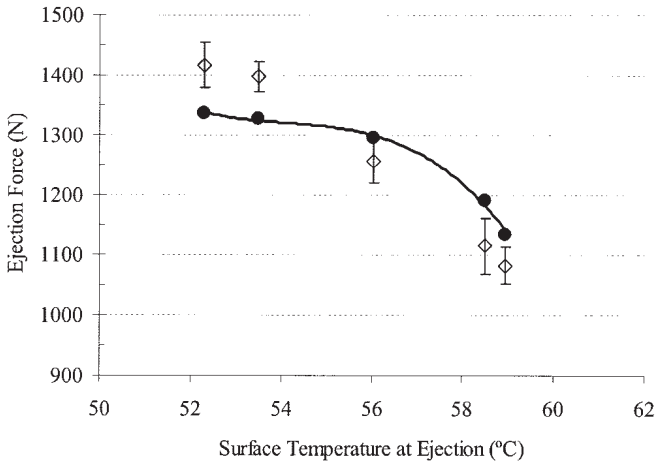

FIG. 5. Comparison of the experimental (symbols) and predicted (line) ejection force for PP. Effect of the surface temperature of the core at ejection.

is dependent on the surface temperature and the roughness of the surface, but data are not yet readily available, in spite of some research being under way [19].

The inclusion of the last term inside the integral depends on the condition of the tube shrinking in the thickness direction. This may happen for lower holding pressures or shorter times leading to the reduction of the force required to eject the part.

Predicting Ejection Force for a Semicrystalline Material

The comparison between the experimental data and the predicted ejection force as a function of the holding pressure is shown in Fig. 4, for the case of the isotactic polypropylene Hifax BA 238 G3 from Montell (MFI = 13 g/600 s (230°C, 21,6 N)).

The effect of the holding pressure on the ejection force is generally in the sense of its reduction with rising the pressure. However, an opposite trend at small holding pressures is observed. This behavior is predicted by the model and is due to two counteracting effects: the volumetric shrinkage increases when the holding pressure decreases, thus contributing to an increase of the ejection force; however, this effect is compensated by an increase of the thickness shrinkage. At higher holding pressures, the reduction of the volumetric shrinkage overcomes the effect of the thickness expansion.

A prediction of the ejection force as a function of the surface temperature of the core was made using the previously referred to thermomechanical model (Fig. 5).

On the basis of the model the decrease of the ejection force with the rise of the surface temperature of the core is an expected result since a concurrent effect of reduction of the modulus and the volumetric shrinkage at ejection points together in that direction.

As can be seen in Figs. 4 and 5, in which the experimental ejection forces and the predictions are compared, in general the model is in close agreement with the experimental data (an average error in absolute value of 4.4% is observed).

Predicting Ejection Force for Amorphous Materials

The comparison between the experimental and the prediction of the ejection force as a function of the holding pressure is shown in Figs. 6 and 7, for two common amorphous materials: polycarbonate (PC Lexan 141R from GE Plastics and polystyrene Lacqrene 1541 from Elf Atochem)

As it can be seen in Figs. 6 and 7, the model agrees generally well with the experimental data. However, some divergence is observed at low and very high pressures. The divergence at low holding pressures is possibly due to an error on the simulated temperatures. This is caused by the detachment of the material from the molding cavity surface, which causes the temperature to remain higher due to the poor heat conduction transfer. The simulation software does not consider this effect. The divergence at high holding pressures is probably caused by the variation of the coefficient of friction being not considered. In fact it is known that the coefficient of friction on the ejection situation of a molding is linked to a replication effect that is likely to be more pronounced at high molding pressures [5, 19].

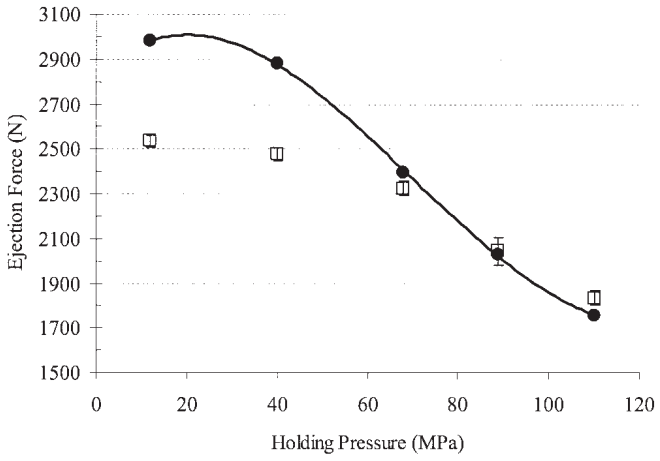

FIG. 6. Comparison of the experimental (symbols) and predicted (line) ejection force for PC. Effect of holding pressure.

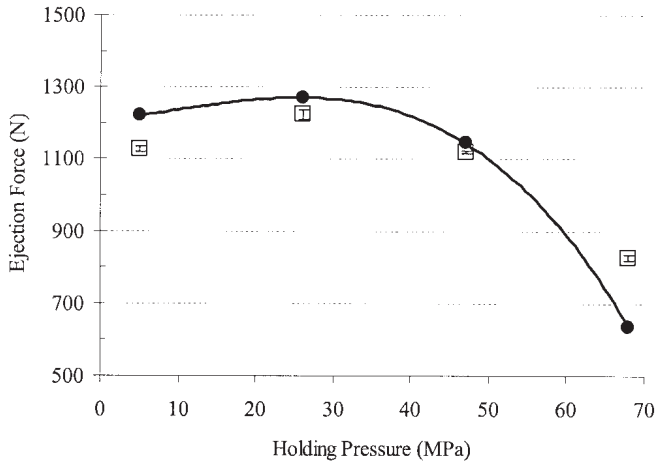

FIG. 7. Comparison of the experimental (symbols) and predicted (line) ejection force for PS. Effect of holding pressure.

A prediction of the ejection force as a function of the surface temperature of the core was also made for polystyrene using the thermomechanical model. In Fig. 8, the predictions are depicted together with experimental data.

As can be seen in Fig. 8, in which the experimental ejection forces and the predictions are compared, in general the model is in close agreement with the experimental data (an average error in absolute value of 1% is observed).

CONCLUSIONS

The injection molding tests were simulated using the software codes C-Mold (for PC and PS) and UNISA code (for PP). The predictions of the temperature profiles and the experimental pressure data were adopted as input to a thermomechanical model for the predictions of ejection forces.

For an isotactic polypropylene, the prediction of the ejection force as a function of the surface temperature of the core using the thermomechanical model is in close agreement with the experimental data. A maximum deviation of 5% between the predicted and experimental data is observed.

For all materials, the thermomechanical model agrees well with the experimental data when the holding pressure is varied.

Some divergence was observed in the case of the amorphous materials (PC and PS), at low holding pressures. This is probably due to the simulated temperatures being calculated by program that does not consider the detachment of the material from the molding cavity surface. This phenomenon causes the temperature to remain higher due to the poorer heat conduction transfer.

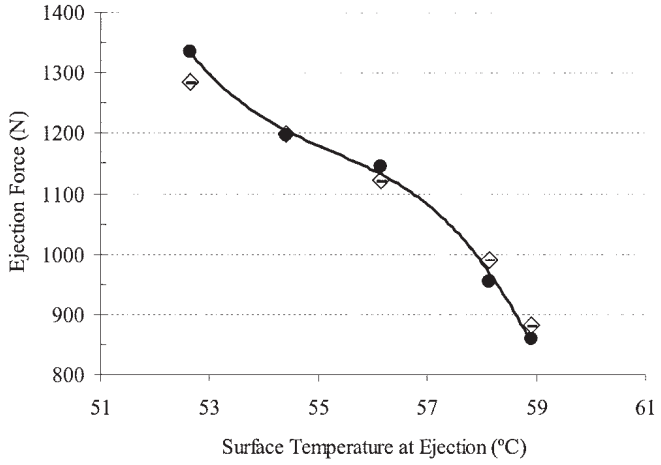

FIG. 8. Comparison of the experimental (symbols) and predicted (line) ejection force for PS. Effect of the surface temperature of the core at ejection.

REFERENCES

1. A. Kaminski, *Kunststoffe*, **66**, 208 (1976).
2. C. Burke and R. Malloy, *Proceedings of the 49th Annual Meeting of the Society of Plastics Engineers*, Montreal, 1781 (1991).
3. A.J. Pontes, G. Titomanlio, and A.S. Pouzada, *Proceedings of the 15th Annual Meeting of the Polymer Processing Society*, Hertogenbosch, paper 330 (1999).
4. G. Menges and P. Mohren, *How to Make Injection Moulds*, Hansen, New York (1993).
5. G. Menges and H. Bangert, *Kunststoffe*, **71**, 13 (1981).
6. H. Wang, K.K. Kabanemi, and G. Salloum, *Polym. Eng. Sci.*, **40**, 826 (2000).
7. K.K. Kabanemi, H. Vaillancourt, H. Wang, and G. Salloum, *Polym. Eng. Sci.*, **38**, 21 (1998).
8. G. Titomanlio and K.M.B. Jansen, *Polym. Eng. Sci.*, **36**, 2041 (1996).
9. K.M.B. Jansen and G. Titomanlio, *Polym. Eng. Sci.*, **36**, 2029 (1996).
10. A.J. Pontes and A.S. Pouzada, *Polym. Eng. Sci.*, **44**, 891 (2004).
11. L.F.A. Douven, F.P.T. Baaijens, and H.E.H. Meijer, *Prog. Polym. Sci.*, **20**, 403 (1995).
12. C.P. Buckley, *Rheol. Acta*, **27**, 224 (1988).
13. F.T.P. Baaijens, *Rheol. Acta*, **30**, 284 (1991).
14. P.P. Benham and R.J. Crawford, *Mechanics of Engineering Materials*, Longman Scientific & Technical, Harlow (1991).
15. S.P. Timoshenko and J.N. Goodier, *Theory of Elasticity*, 3rd ed., McGraw-Hill, New York (1970).
16. A.J. Pontes, A.M. Brito, and A.S. Pouzada, *J. Injection Molding Technol.*, **6**, 343 (2002).
17. G. Titomanlio, V. Speranza, and V. Brucato, *Int. Polym. Process*, **12**, 45 (1997).
18. *C-Mold 99.7 User's Guide*, Moldflow, Ithaca, NY (1999).
19. E.C. Ferreira, N.M. Neves, R. Muschalle, and A.S. Pouzada, *Proceedings of the 59th Annual Meeting of the Society of Plastics Engineers*, Dallas, 1546 (2001).